LAWRENCE
LIVERMORE
NATIONAL
LABORATORY

LLNL-JRNL-471526

A New Method to Generate Dust with Astrophysical Properties

J. F. Hansen, B. Breugel, E. M. Bringa, B. Eberly, G. A. Graham, B. A. Remington, E. A. Taylor, A. G. G. M. Tielens

February 25, 2011

Journal of Instrumentation

Disclaimer

Not to appear in Nonlearned J., 45.

A new method to generate dust with astrophysical properties

J. F. Hansen,[1] W. van Breugel,[2] E. M. Bringa,[3] B. Eberly, G. A. Graham,[4] and B. A. Remington

Lawrence Livermore National Laboratory, Livermore, CA 94550

hansen46@llnl.gov

E. A. Taylor[5]

The Open University, PO Box 197, Milton Keynes MK7 6BJ, UK

and

A. G. G. M. Tielens

Leiden Observatory, Leiden University, PO Box 9513, NL-2300RA Leiden, The Netherlands

ABSTRACT

To model the size distribution and composition of interstellar and interplanetary dust grains, and their effect on a wide range of phenomena, it is vital to understand the mechanism of dust-shock interaction. We demonstrate a new experiment that employs a laser to subject dust grains to pressure spikes similar to those of colliding astrophysical dust, and that accelerates the grains to astrophysical velocities. The new method generates much larger data sets than earlier methods; we show how large quantities (thousands) of grains are accelerated at

[1]General Atomics, San Diego, CA 92121

[2]Office of Undergraduate Education & School of Natural Sciences, University of California, Merced, CA 95343

[3]CONICET & Instituto de Ciencias Basicas, Universidad Nacional de Cuyo, Mendoza 5500, Argentina

[4]Mineralogy Department, The Natural History Museum, London SW7 5BD, UK

[5]MMI Engineering Ltd., Warrington WA4 6HL, United Kingdom

once, rather than accelerating individual grains, as is the case of earlier methods using electric fields. We also measure the in-flight velocity ($\sim 4.5\,\mathrm{km/\,s}$) of hundreds of grains simultaneously by use of a particle image velocimetry (PIV) technique.

Subject headings:

1. Introduction

In this manuscript we present a new technique that can be employed to accelerate dust grains to hyper-velocities, and that subjects the dust grains to the short pressure spikes seen in grain-grain collisions in interstellar space. This new technique can become a useful tool for research on both interstellar dust grains and on hyper-velocity impacts of dust grains on space hardware. We also present the first ever particle imaging velocimetry (PIV) measurements in a dusty plasma where the dust grains are moving at hyper-velocities (several km/s).

The presence of dust in the interstellar medium of galaxies is very apparent through extinction of stellar and nebular photons, through scattered light, through optical and infrared polarization, and through infrared emission (1). Interstellar dust controls the appearance of galaxies ranging from far-ultraviolet to far-infrared and sub-millimeter wavelengths. Our understanding of astronomical observables requires proper correction for foreground dust extinction.

Dust also plays an active role in the Universe. The extinction of starlight in dense clouds allows molecules to survive. Even more importantly, grains provide surfaces where catalytic reactions can convert simple molecules into complex ones (2). Small interstellar dust grains are the building blocks of planetesimals, cometesimals, and larger planetary bodies in disks surrounding young protostars. Through its influence on the chemistry of molecular clouds, dust also affects the cooling of dense gas and thereby sets the point when gravitational forces can overcome supporting thermal forces. Many of the key processes that drive the evolution of galaxies – including star and planet formation and accretion onto central black holes – occur deeply inside dust-enshrouded regions. Consequently, understanding dust is crucial to understanding astrophysics, astrochemistry and astrobiology, including the molecular inventory of regions of star and planet formation.

The role of dust in space depends very much on the detailed characteristics of the dust, including its structure, composition, and, in particular, its size distribution. While these properties are initially set by the processes in the atmospheres of dying stars where interstellar dust is born, many processes influence them thereafter. Processing by strong

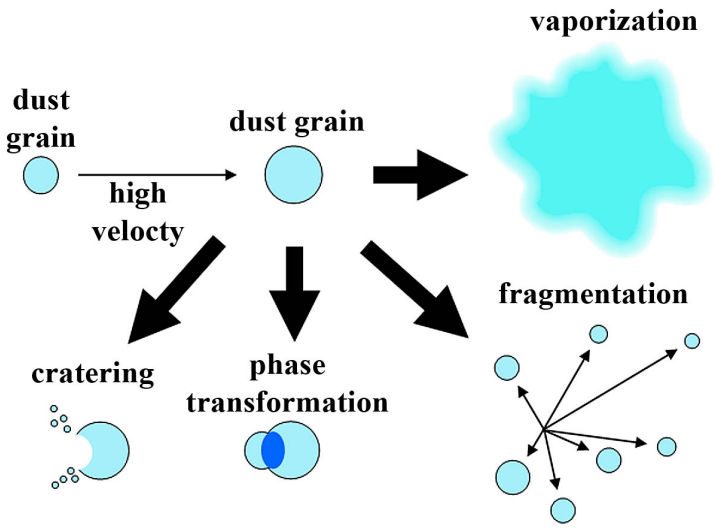

Fig. 1.— A grain-grain collision can result in (depending on the kinetic energy, material properties, and grain sizes involved) cratering, phase transformation, fragmentation, or vaporization.

shock waves driven by supernova explosions are of particular importance in this regard (3; 4; 5; 6; 7; 8; 9). Theoretical studies for the processing of dust grains in these environments have paid most attention to the effects of energetic ions returning solid material to the gas phase. Sputtering is of great importance in material sciences, driving for example the semi-conductor industry, and the numerous experiments and theories in this field have been instrumental in the development of detailed models for sputtering under astrophysically relevant conditions (10). However, grain-grain collisions are of equal importance in astrophysical shocks (9) and, in contrast, very little experimental data or theoretical studies are available on size scales (sub-micron) that are of relevance in space (10).

In particular, grain-grain collisions dominate the evolution of the interstellar grain size distribution and composition of astrophysical dust grains (9). The processes that occur during grain-grain collisions (7; 9) at very high relative velocities, are illustrated schematically in Fig. 1. Shattering by collisions affects the grain size distribution and total surface area available for, for example, chemical reactions. In addition, the grain composition and structure can be altered through phase transitions. As an example, one intriguing aspect is the "diamonds in the sky" prediction, whereby graphite grains are suggested to be transformed into diamonds in the strong shocks induced in grain-grain collisions (5). Adding support to this hypothesis was the discovery of small diamond grains ($\sim 50\,\text{Å}$) in carbonaceous meteorites, with a presolar origin suggested by the isotopic composition of trapped noble gases

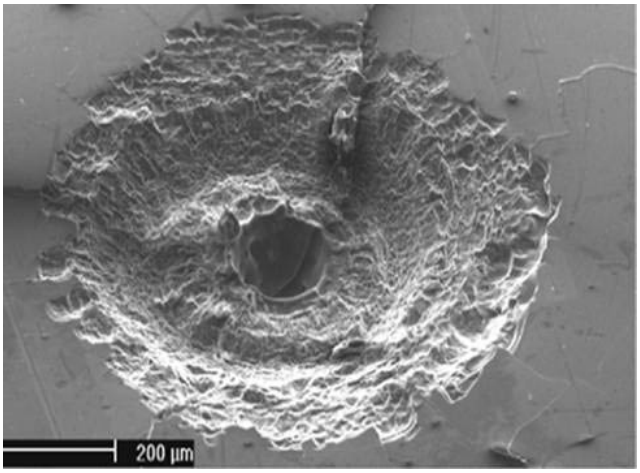

Fig. 2.— A scanning electron microscope (SEM) image of a crater on one of the solar panels of the Hubble Space Telescope. [Image courtesy Giles Graham.]

(11). The shock strengths required are high, $p_{shock} > 500\,\mathrm{kbar}$, but their durations are fleetingly short, a few picoseconds, and the spatial scales of the grains are sub-micron. Under these conditions, it is not even known whether carbon can be transformed to diamond, as suggested. This prediction can be tested experimentally, provided the required pressure, spatial, and temporal scales can be reproduced.

Closer to home, micrometeorites and hypervelocity (> 1 km/s) interplanetary dust particles (IDPs) present a hazard to space flight and are a source of damage and failure to space hardware. Space-based hardware (solar panels, thermal shields, etc.) needs to be designed to operate for extended exposures in space, which means exposures to the presence of hypervelocity impacts of IDPs. Solar panels and other hardware from, for example, the Hubble Space Telescope (HST), that have been returned to Earth, exhibit very clearly the effects (cratering, micro-cracking, and other localized damage spots) of these IDP particle impacts (12; 13; 14; 15; 16; 17; 18; 19). An example is shown in Fig. 2. An enduring puzzle, however, is why no impact craters smaller than $\sim 10\,\mu$m are observed. The predicted IDP grain size distribution (1) suggests that the incident flux should in fact be largest for the smallest grains, and crater size should scale as some power of incident particle kinetic energy. Yet, there is little evidence of lower-kinetic energy impacts. Either the models for the size distribution of the incoming flux of IDPs are in error, or the effect of their impacts is not properly understood. This question can also be addressed experimentally, where the impactor mass and velocity can be controlled independently and varied over a considerable range.

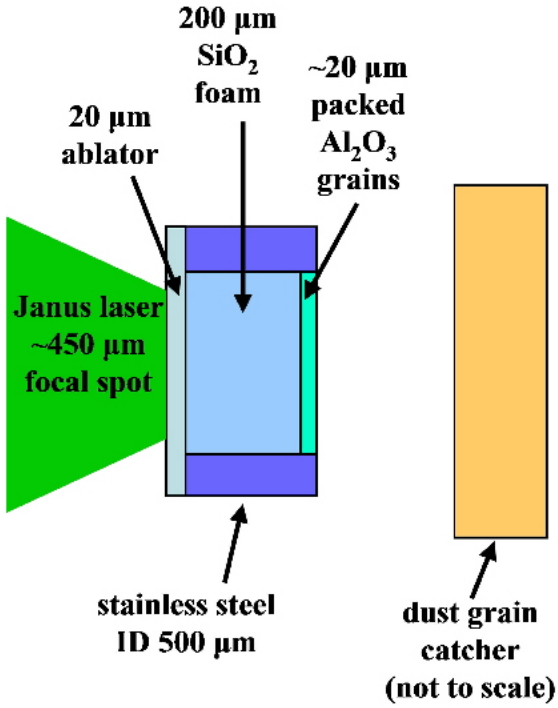

Fig. 3.— Target design: a 220 μm thick stainless steel target substrate with a 500 μm diameter hole is filled with aerogel. Coated on "top" of the target substrate (to the left in this image) is a $\sim 20\,\mu$m thick ablator. The "bottom" of the hole (to the right in this image) contains a layer of Al_2O_3 grains with diameters $\leq 5\,\mu$m. In this work the layer thickness was nominally 20 μm, although ideally the layer thickness would be that of a single dust grain.

2. Experiment design

We invented and tested a new laser-based laboratory capability to carry out experiments on the shock processing resulting from grain-grain collisions, and the damage and cratering of space hardware due to hypervelocity IDP impacts. To this end, we designed a laser target containing a collection of dust grains as shown in Fig. 3. In this design, a laser illuminates a solid-density ablator $\sim 20\,\mu$m thick, launching a strong shock that moves through the $0.1\,\mathrm{g/cm^3}$, $\sim 200\,\mu$m thick foam reservoir. At the back side of this reservoir are the dust particles of interest, many microns to sub-micron-size spheres of graphite, diamond, or other materials of interest to interstellar dust dynamics. As the shock releases at the back side of the reservoir the duration of high pressure conditions on the grains would be very short.

To guide the design, we show in Fig. 4 the results from numerical simulations in 1D using the HYADES radiation hydrodynamics code (20). (In this approximation, the grains

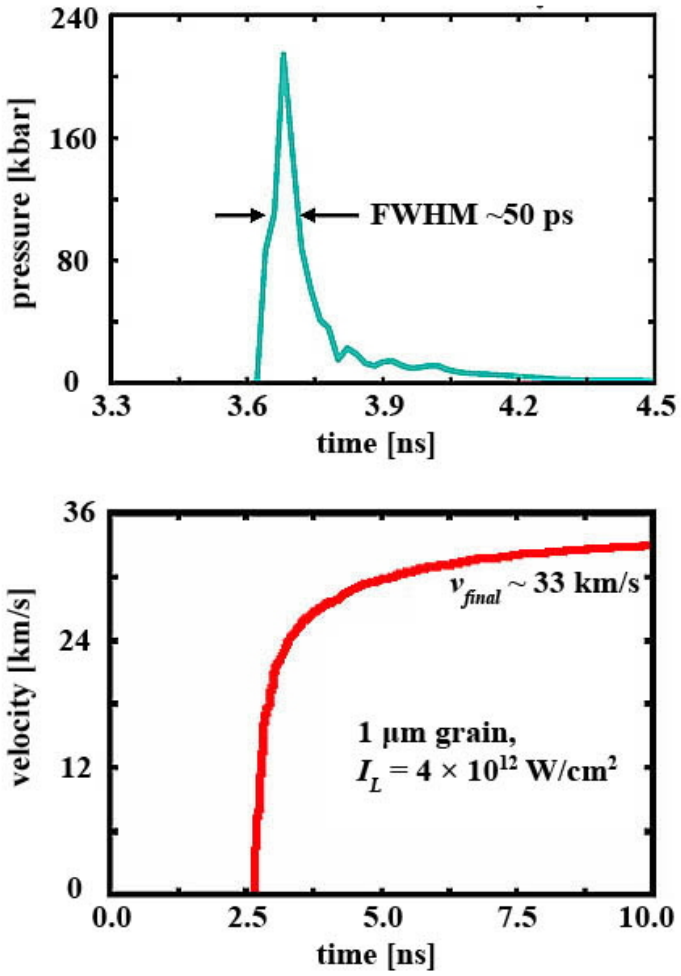

Fig. 4.— Pressure (*top*) and velocity (*bottom*) histories of a dust grain at the rear surface of the laser target as calculated in 1D HYADES simulations.

are treated as a 1D very thin foil.) It is clear that we can control both the magnitude of the pressure spike from the shock and its duration in the dust grains. Figure 4 (top) shows pressure versus time inside a graphite grain. The predicted dwell time (high pressure interval) is 50 ps or less. This is an over-estimate, due to the effect of artificial viscosity in the hydrodynamics code (a common numerical "trick" to artificially spread out the shock discontinuity over several zones). A more time consuming MD simulation would give a considerably shorter, more realistic dwell time; for comparison see Fig. 6, which shows MD simulations albeit for smaller dust grains.

Figure 4 (bottom) shows a predicted micro-impactor velocity of $\sim 33\,\mathrm{km/s}$. This is likely an over-estimate by the 1D code, and corresponds better to the final velocity of the ex-foam plasma than the final velocity of a dust grain. In a real 3D environment, the final plasma velocity will be slightly less ($\sim 25\,\mathrm{km/s}$ may be a reasonable estimate based on our experience with 2D and 3D codes) and some plasma will slip past the grain instead of pushing it, so that the final grain velocity will be reduced by a factor of a few.

A better estimate of the final grain velocity can be obtained by considering a viscous drag model. The drag force on a sphere with diameter h in a fluid with velocity U is:

$$F_D = C_D \frac{1}{2} \rho \left(U - v\right)^2 \frac{\pi}{4} h^2 \tag{1}$$

where C_D is the drag coefficient, ρ is the fluid density, and v is the velocity of the grain (measured in the same reference frame as U). Use Newton's second law and simplify:

$$\frac{3}{4} C_D \rho \left(U - v\right)^2 = h \rho_s dv/dt \tag{2}$$

where ρ_s is the grain density. The drag coefficient C_D is a complicated function of the Reynold's number $\mathrm{Re} = h\left(U - v\right)/\nu$, and U, ρ, and ρ_s are all functions of both time t and position x, so Eq. 2 requires a numerical solution to be solved exactly. However, we note that the ratio ρ/ρ_s varies much less than does either ρ or ρ_s on its own, and that a constant U is a fairly reasonable approximation as the fluid velocity reaches within 10% of its final value in just a couple of nanoseconds (see Fig. 4). If also C_D is constant, then Eq. 2 can be solved explicitly for the grain velocity as a function of time t:

$$v = U - \frac{1}{Kt + \frac{1}{U}} \tag{3}$$

and implicitly for the grain velocity as a function of the grain travel distance x:

$$x = \frac{v}{K\left(U - v\right)} - \frac{1}{K} \ln\left(\frac{U}{U - v}\right), \tag{4}$$

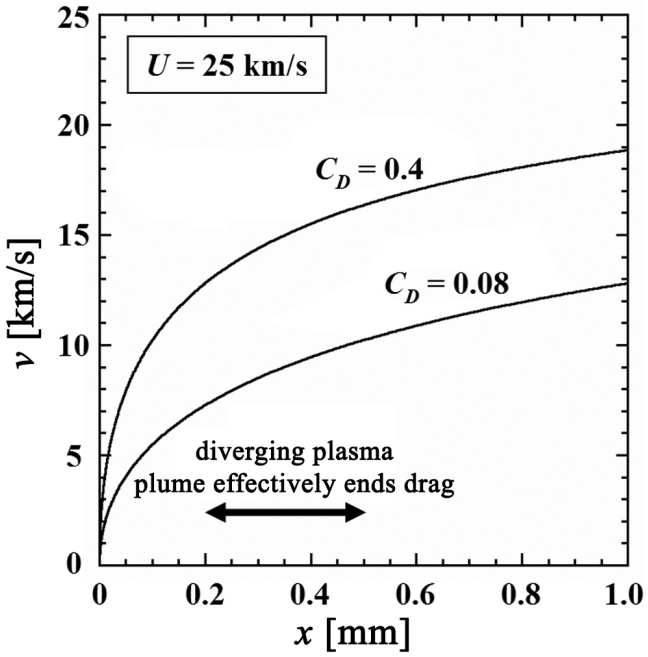

Fig. 5.— Velocity as a function of distance traveled for a 5 μm diameter Al_2O_3 dust grain surrounded by a 25 km/s plasma flow, for two different drag coefficients: $C_D = 0.08$ (turbulent flow) and $C_D = 0.4$ (laminar flow). In the experiment, the drag force decreases due to a diverging plasma plume, effectively ending acceleration somewhere between $x \approx 0.2$ mm and 0.5 mm (and reducing it prior to $x = 0.2$ mm).

where we have defined a constant

$$K \equiv \frac{3}{4}\frac{1}{h} C_D \frac{\rho}{\rho_s}. \tag{5}$$

In actuality C_D is not constant, but we can find limits on C_D and thus bounds on the grain travel distance in Eq. 4. To find the limits on C_D, we must first establish the range of Reynolds numbers experienced by a dust grain. Initially the velocity difference $U - v$ between flow and grain is quite large, and the Reynolds number (calculated using a viscosity ν based on Clerouin's model (21; 22)) is in the interval $4.5 \times 10^5 < \mathrm{Re} < 8.5 \times 10^5$ corresponding to a turbulent flow with $0.08 < C_D < 0.15$ (23). Later, as the grain gains some speed, the Reynolds number may drop below 3×10^5, which could stabilize the flow in a laminar state with $C_D \approx 0.4$. In short, the drag coefficient must must be in the interval $0.08 < C_D < 0.4$ for any Re of interest in the experiment. We can calculate two solutions, one for $C_D = 0.08$ and one for $C_D = 0.4$, and know that the real solution lies somewhere in between these (and likely close to the solution for turbulent flow with $C_D = 0.08$).

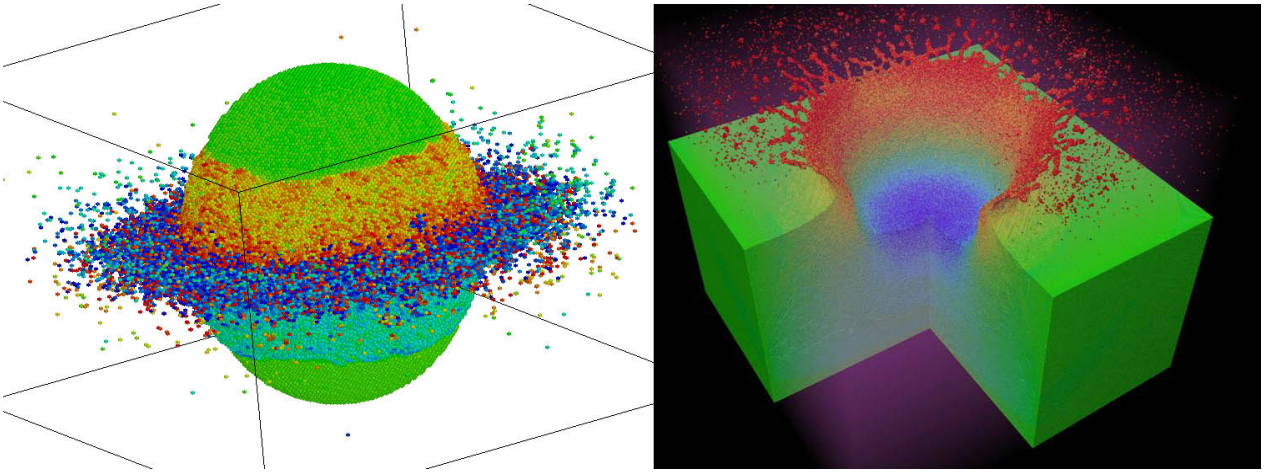

Fig. 6.— Two molecular dynamics (MD) simulations: *Left:* a grain-grain collision of the type that might be found in the flux of interplanetary dust. The relative impact velocity was 7 km/ s and the dust particles were 18 nm diameter Cu spheres. The resulting pressure spike felt by the Cu "dust grain" is ~ 200 kbar in magnitude with a duration $t_{FWHM} \approx 5$ ps. *Right:* a 20 nm grain 20 ps after impacting a slab of material creating a crater. In both images, color represents potential energy (PE): bright red and dark blue mean high PE, that is, large disorder. Green represents the PE minimum of the initial crystalline state. These MD simulations are state-of-the-art, yet very uncertain. They can be tested with the experiments that we have begun. [MD simulation courtesy Eduardo Bringa.]

Equation 3 shows that the grain velocity $v = 0$ at $t = 0$ and then $v \to U$ as $t \to \infty$, as expected. Equation 4 is more practical in that it gives us a relation between grain position and grain velocity; in the 3D experiment, the plasma diverges behind the target in a plume, reducing the drag on the grain. This effect occurs over a length scale comparable to the characteristic dimensions of the target. Two solutions of Eq. 4 (for $C_D = 0.08$ and $C_D = 0.4$) are shown in Fig. 5. The final dust grain speed for this target could be up to $\sim 7 - 10$ km/ s taking into account the diverging plume. Higher velocities could be achieved using a larger laser (such as the National Ignition Facility), which can drive a larger target.

3. Experiment set-up and diagnostics

Based on the design and analysis above, we assembled nine targets for experiments. Each target consisted of a piece of 220 μm thick stainless steel with a drilled 500 μm diameter hole filled with aerogel. The "bottom" of the hole contained a layer of ≤ 5 μm diameter Al_2O_3

grains. The layer thickness was typically 20 μm - thicker than the design value but deemed adequate for a first experiment and with increased chance of success for our diagnostics (described below) - and there were individual variations between each target (see Fig. 7). Coated on top of the shim stock was an ablator consisting of a 25.5 μm thick layer of parylene-C - slightly thicker than the 20 μm design value - followed by a flash coating of $\sim$ 1000 Å Al.

The experiment was set up in the vacuum chamber of Target Room 1 at the Jupiter Laser Facility (24), using one beam of the Janus laser to drive the target. The experiment set-up is shown in Figs. 8 and 9. The drive laser wavelength was 527 nm and the laser pulse length was 5 ns. The laser energy varied from shot to shot but was typically 200 J. A 25 mm by 50 mm Cu foil was placed 25 mm behind the target to catch hyper-velocity grains. The foil was 125 μm thick, 99.9% pure, "half hard" Cu, and was backed by a thicker piece of Cu.

A probe laser (also with a 527 nm wavelength) was sent via a series of mirrors and a cylindrical lens (with focal length 500 mm) to illuminate the area right behind the target with a laser sheet. The probe beam also passed through a beam-splitter pair, temporarily creating two legs of the laser, with equal laser energies, before recombining the beam paths again. One leg was much longer than the other, creating a 40.18 ns delay between the two laser pulses. The laser energy was $100 - 150$ mJ per pulse (i.e., requiring a laser energy of $400 - 600$ mJ prior to the beam splitters).

An imaging system was set up to image Mie-scattered laser light coming off dust grains as they fly toward the grain catcher. The imaging system was set up in a microscope configuration with three doublet achromet lenses in the objective and a Hastings triplet achromat in the ocular, as shown in Fig. 9. Also in the beam path were a glass blast shield (to protect the objective), two high-quality, AR-coated, wedged vacuum chamber windows, and a 527 nm linepass filter (primarily with the purpose of blocking infrared plasma glow). The objective had a light gathering capability equivalent to $f \sim 1.8$, which combined with the requested laser energy was predicted to provide enough light to observe the dust grains. The ocular focused images on a gated MCP backed by a 512×512 pixel CCD with a pixel size of 19 μm. The ocular had a magnification of either 5.9× or 8.8× (two configurations were tried), creating images with either 310 or 465 pixels per mm object space (and thus had a field of view 1.65 mm or 1.10 mm, respectively). The magnification and resolving power of the optical system is demonstrated in Fig. 10.

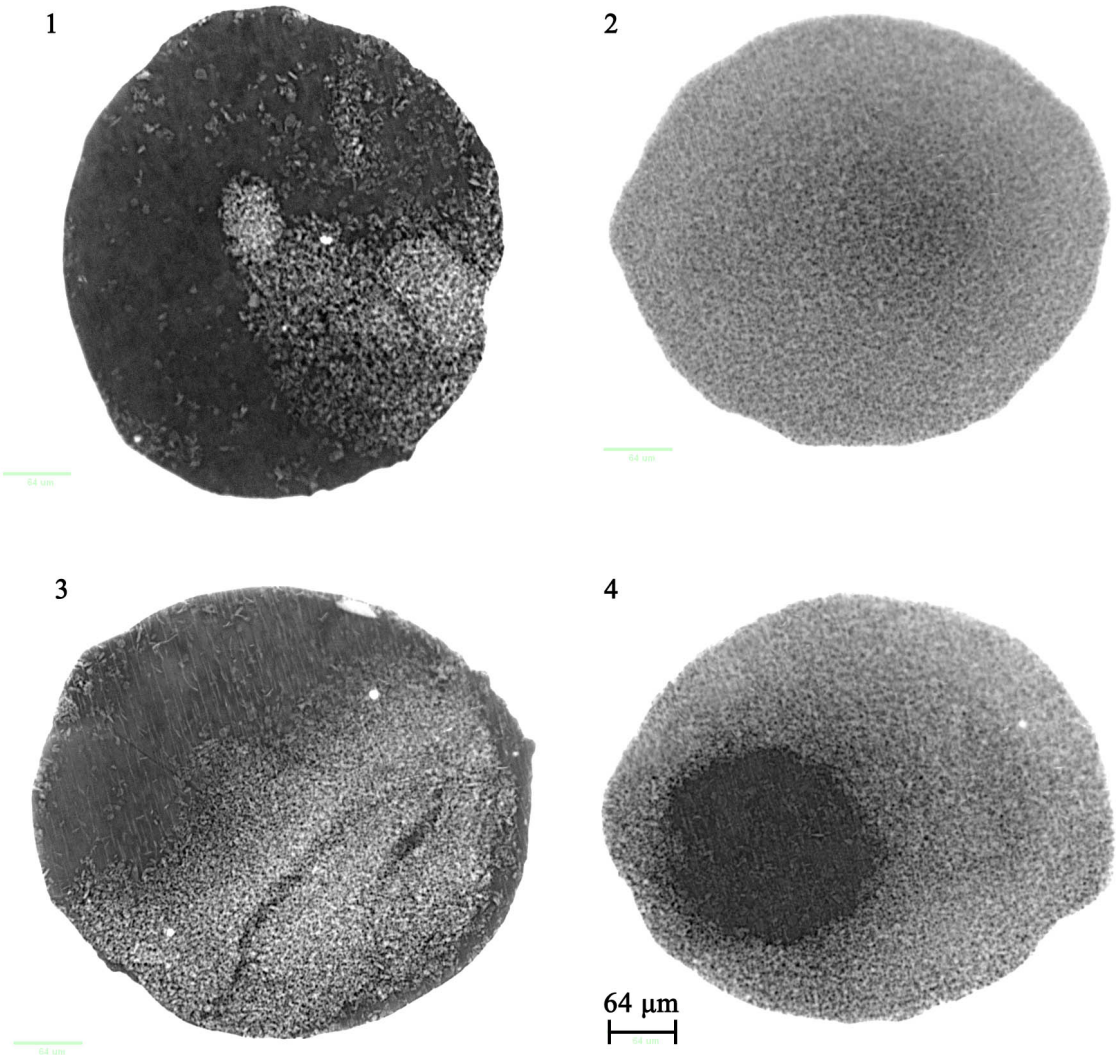

Fig. 7.— X-ray metrology images of four targets looking through the 500 μm hole in the stainless steel substrate. The grain coverage over the hole varies from target to target; bright areas contain Al_2O_3 grains, while dark areas are free of grains.

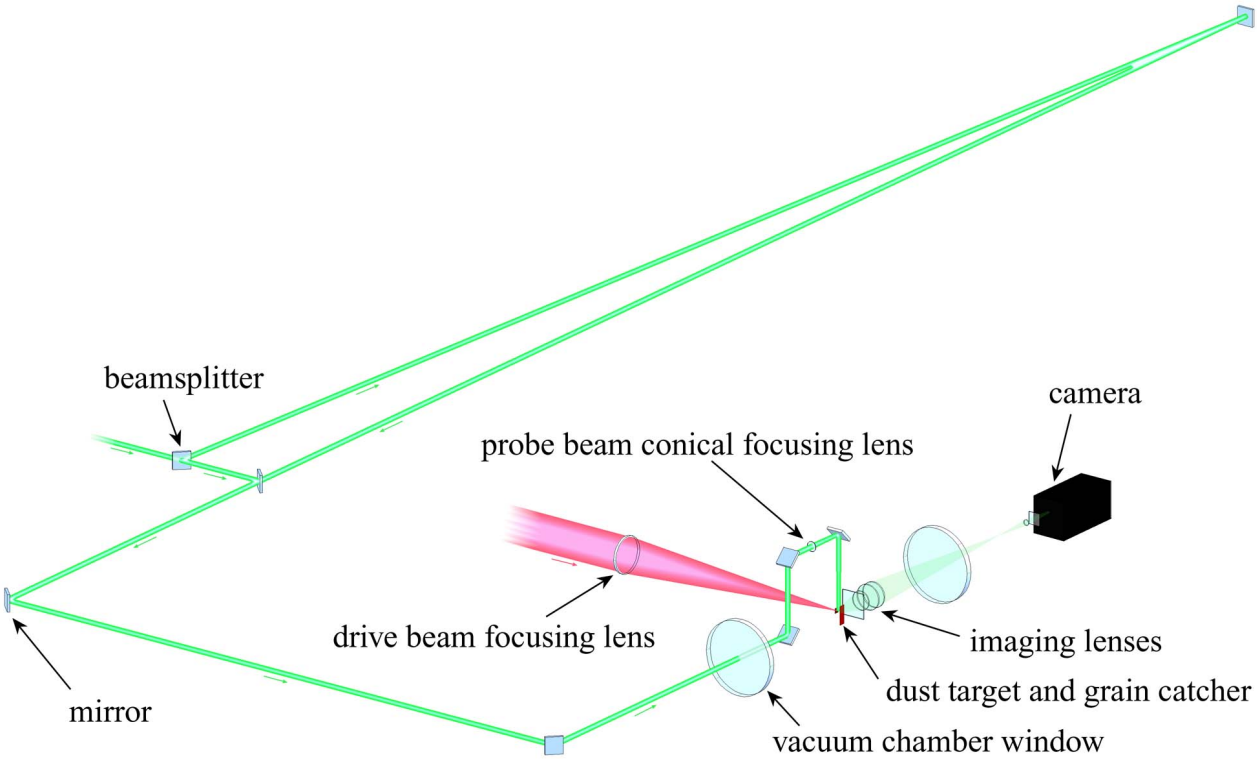

Fig. 8.— The experiment set-up consists of three major elements: (I) The laser drive beam, target, and dust grain catcher, all in line; (II) a probe beam laser with a set of beam-splitters, mirrors and a cylindrical lens to create a laser sheet to illuminate the dust grains in flight; (III) an imaging system.

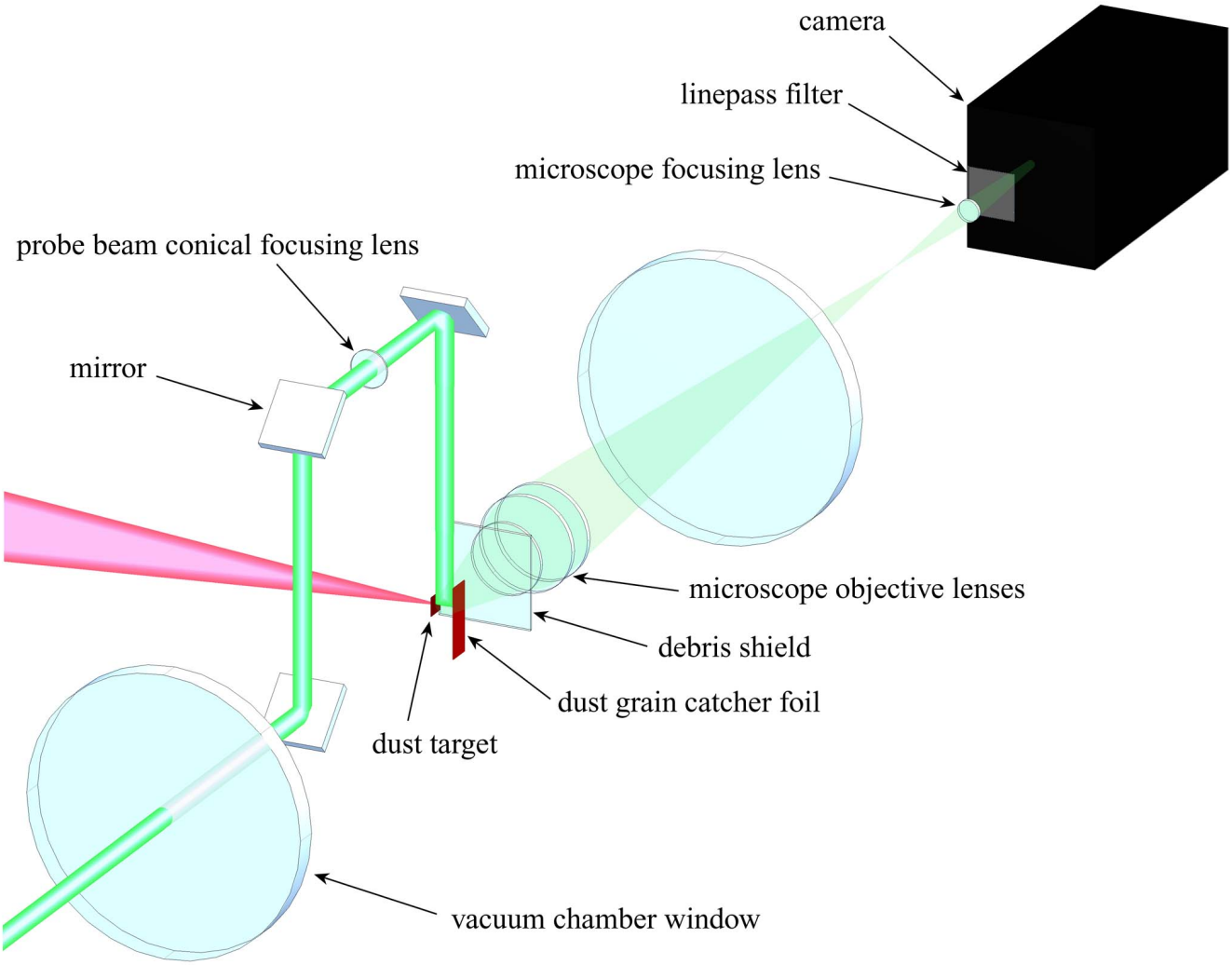

Fig. 9.— A close up of the experiment's target area. The imaging system functions like a microscope and consists of four lenses (three doublet achromats in the objective; one Hastings triplet in the focusing ocular), a 527 nm line-pass filter, and a gated camera.

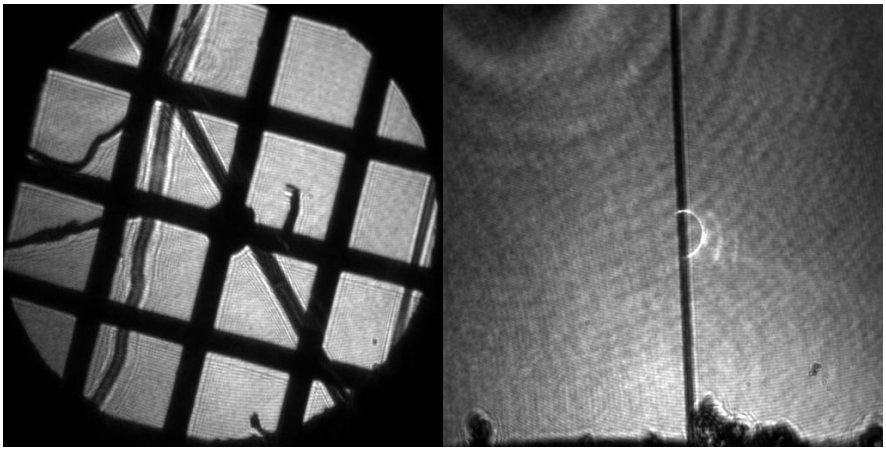

Fig. 10.— *Left:* The microscope imaging system was focussed using an alignment target with a square grid pattern. The size of the squares (each side is 250 μm) was used to verify the magnification. *Right:* The resolving power of the system was verified by imaging an 8 μm diameter fiber. The bright arc in the center is a lens flare.

4. Experimental results

We successfully obtained experimental images of seven of nine targets, with an example shown in Fig. 11. Dust grains appear in many of these images as elongated shapes, longer in the horizontal direction than in the vertical direction as the grains are moving right to left. We can estimate the grain velocity by measuring the size of this elongation. This is a type of particle image velocimetry (PIV) technique. Dust grains near the vertical center-line of Fig. 11 (left) are roughly 8 pixels wide by 4 pixels tall. This means the grain is moving at a speed of

$$\frac{\frac{8\text{ pixels}-4\text{ pixels}}{310\text{ pixels/mm}}}{5\,\text{ns}} = 2.6\,\text{km/s}.$$

Dust grains toward the left edge of the image are more elongated, roughly 11 pixels wide by 4 pixels tall, which corresponds to a velocity of 4.5 km/ s. These values are in good agreement with the limits set by when and where we obtained the image; the image was taken some 3 mm behind the target 1 μs after the drive laser fired. Had a grain been moving at a constant velocity during this time, it would have to move 3 km/ s to end up in the center of the image. Since the field of view of the image is 1.65 mm, a grain would have to move with a constant velocity in the range 1.4 km/ s to 4.6 km/ s to be within the boundaries of the image. The cause of the velocity spread is the original thickness of the dust layer; had the dust grain layer not been more than one grain thick, the velocity spread should have narrowed considerably by the removal of the slower grains. This suggests that fewer grains should be used in future

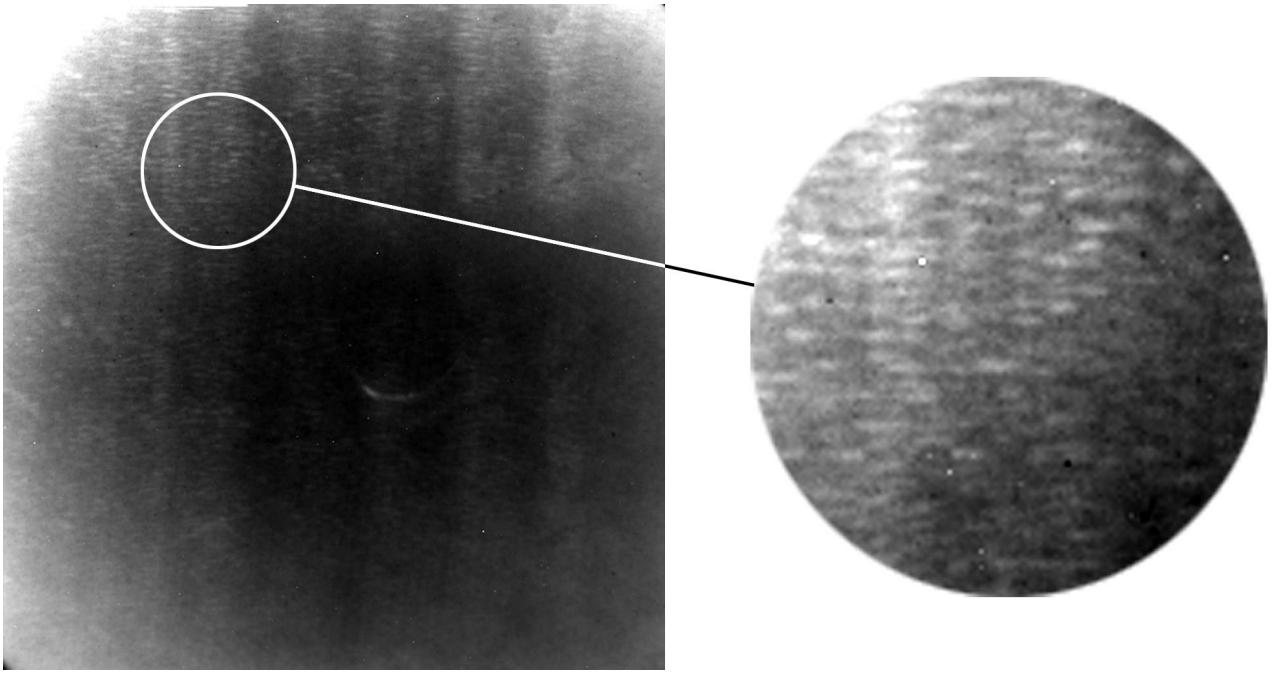

Fig. 11.— *Left:* This image has a field of view of 1.65 mm and shows hundreds of dust grains in flight, traveling from the target substrate (located ~ 2.2 mm to the right and outside of the image boundary) toward the grain catcher (a Cu foil some 21 mm to the left). *Right:* In this magnification of a section of the image, it is clear that the grains are elongated horizontally due to motion blurring. The elongation indicates a speed of a few km/s.

experiments. However, as it were, the measured velocities in the experiment are in good agreement with the calculated velocities in the design analysis.

The splitting of the probe beam into two separate pulses was done so that each dust grain would be recorded twice in each image. The separation between the two locations divided by the time separation of the laser pulses would then give a very precise measurment of the grain velocity (this is a well-established PIV technique used in the "dusty plasma" community employed to image micron-sized dust grains carried by magnetized plasmas typically at a few mm/ s (25)). However, in our images we see so many grains that it is difficult to identify grain "pairs." With some effort it is possible that pairs can be identified and a more accurate PIV analysis can be conducted, and in future experiments with fewer grains, this should be easier.

Each of the nine targets produced craters on a Cu grain catcher foil. Viewing the foils with a scanning electron microscope (SEM) reveals a spectacular amount of craters. This

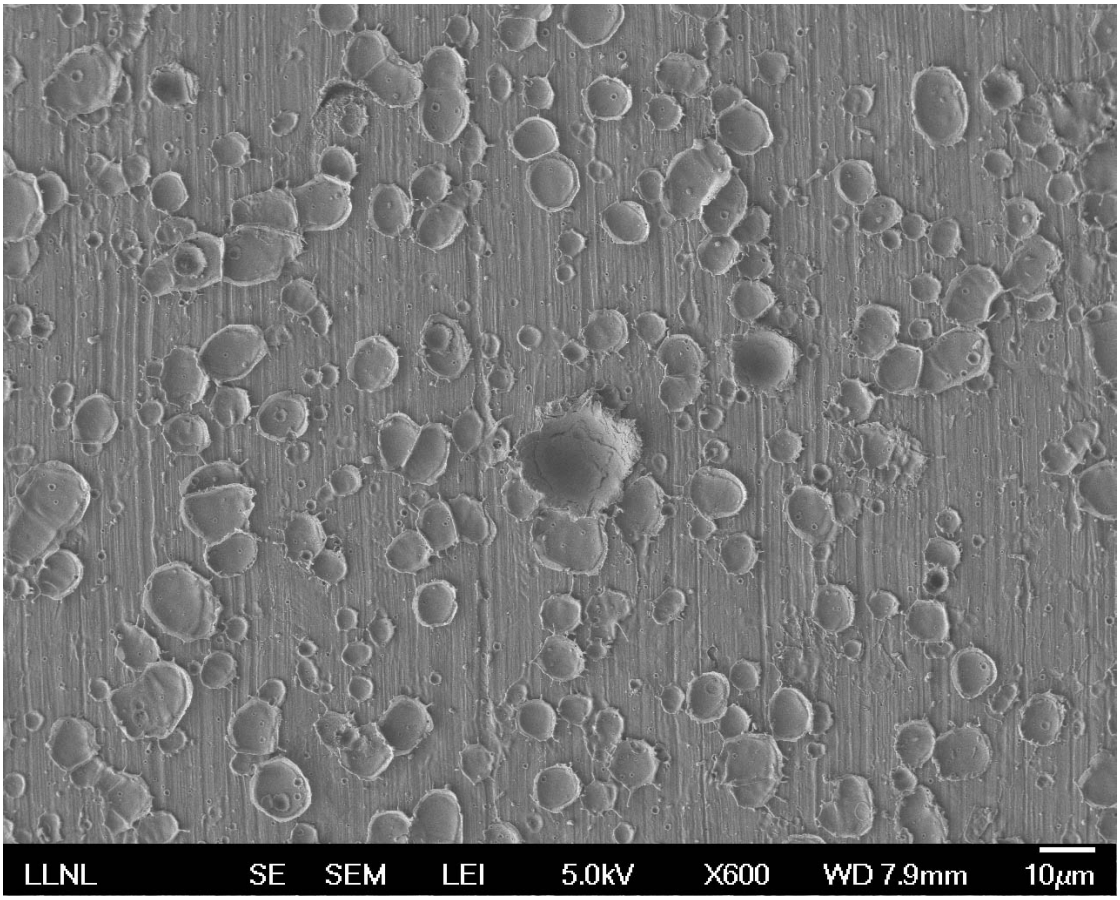

Fig. 12.— Image of a cratered Cu foil grain catcher showing an abundance of craters. [The image is a lower secondary electron image (LEI) produced by a scanning electron microscope (SEM) at 600× magnification.]

is readily seen in the low magnification of Fig. 12. This result also suggests that we could have used fewer dust grains. Fortunately, most craters appear to be single impacts, caused by a single impactor. Some the craters are "classic" craters and some are shallower "splash" craters. Many craters contain traces of Al and O, which can reasonably only be due to grain impacts (see Fig. 13). These craters are not much bigger than 5 μm in diameter, which also suggest they came from dust grain impacts. In some areas of the Cu foils, other craters show traces of Fe (see Fig. 14), likely due to impacts of steel droplets coming from the melting and erosion of the target hole walls. Thus, selecting a material for the target substrate that was different from the dust grain composition was important, because it allows us to exclude from our analysis the foil regions where some cratering is due to substrate droplets.

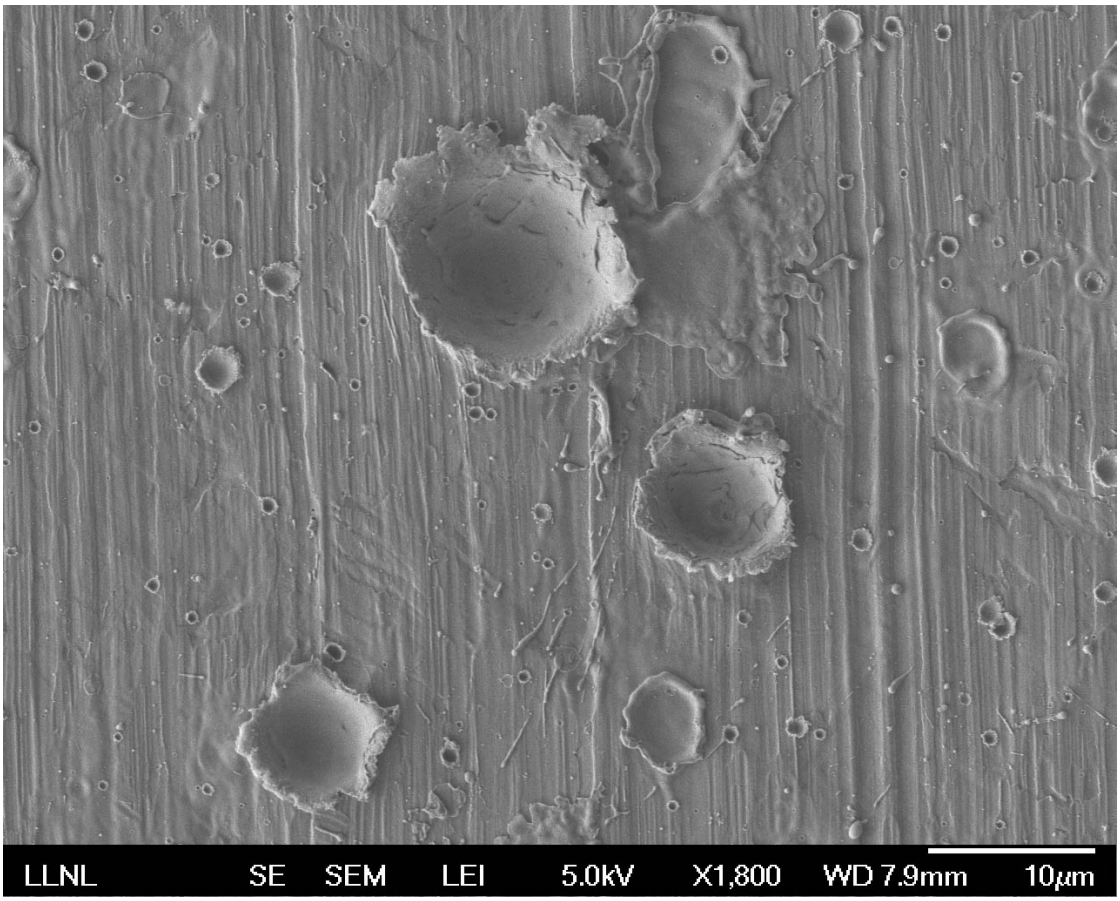

Fig. 13.— Another section of the same Cu grain catcher foil with examples of craters containing Al and O, presumably due to grain impacts. [The image is a lower secondary electron image (LEI) produced by a scanning electron microscope (SEM) at 1800× magnification.]

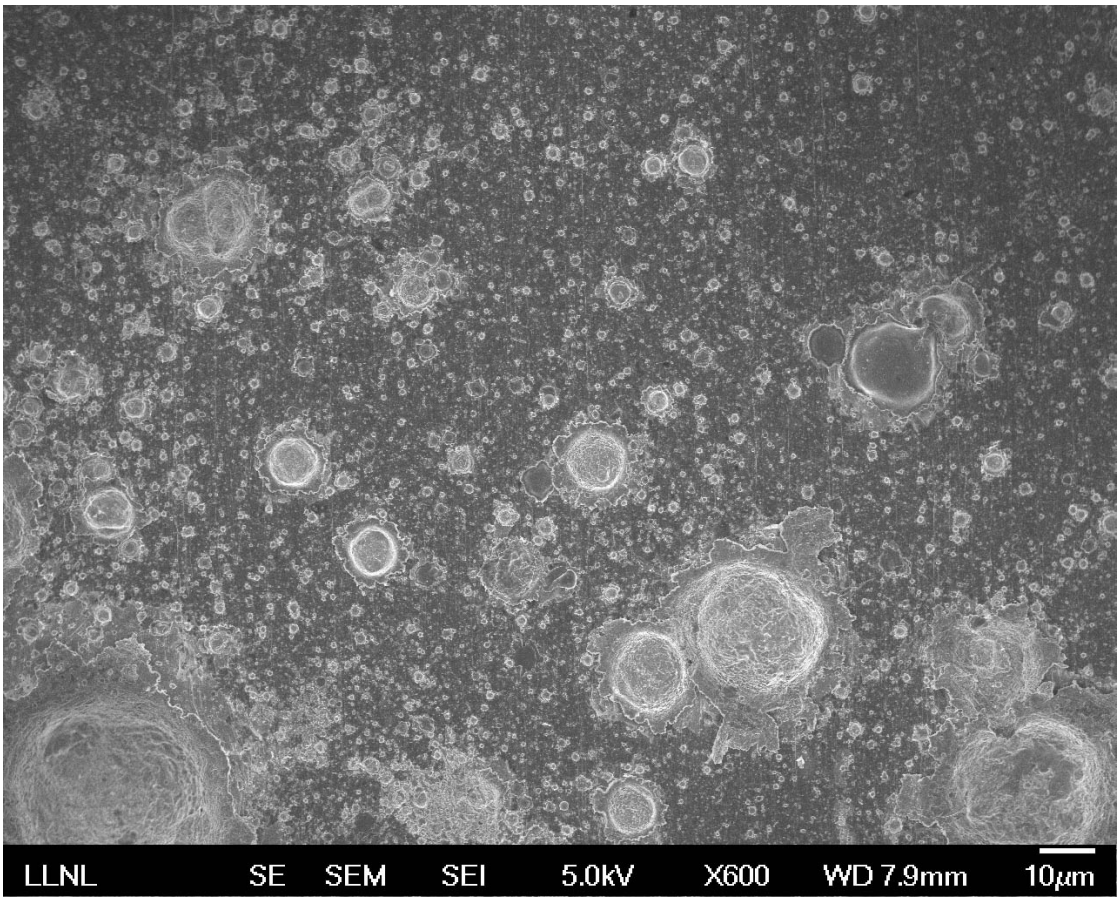

Fig. 14.— The craters shown here contain Fe, suggesting they were caused by impacts of droplets coming off the target hole walls. [The image is a secondary electron image (SEI) produced by a scanning electron microscope (SEM) at 600× magnification.]

5. Conclusions

Using a new laser-based laboratory capability, we have subjected dust grains to pressure spikes similar to those of astro-physical dust processing, and have accelerated the dust grains to hyper-velocities. The dust grain composition in our experiment was Al_2O_3, but the new technique presented here should be tunable to diamond grains, "aggregate grains," and other grains of astrophysical interest, to study phase transitions and changes in grain size distribution. We have measured the resulting grain velocity to be at least 4.5 km/ s, consistent with a theoretically derived value. The measurement was done by employing a PIV technique similar to what is used in the "dusty plasma" community, but at speeds some 5 to 6 orders of magnitude higher.

We also showed that the hyper-velocity grains caused cratering on a Cu foil in our experiment, and that the cratering can be analyzed using scanning electron microscopes. Replacing the Cu foil with actual space hardware is easily accomplished, and a range of projectile grain sizes and velocities could be used, allowing the hardware surfaces to be examined for cratering and thermally driven micro-cracking. The dust grains can also be captured gently in aerogels, reproducing the methodology of the recent Stardust mission (26) and building on the experience of extracting and characterizing micrograin materials impacted into SiO_2 aerogel (15; 19). Observables to look for in future experiments include whether these shock processed micrograins (1) melted and refroze, or remained solid throughout, (2) fractured or remained whole, (3) suffered severe plastic flow, or remained largely elastic, i.e., retained their original shape, and (4) whether graphite micrograins transitioned to and remained in the diamond phase on this short time scale (27). The experimental data could then be compared to state-of-the-art molecular dynamics simulations (28; 29; 30) for single grain collisions.

The authors would like to thank Dr. Edward Thomas, Jr. at the Auburn University Plasma Sciences Laboratory for sharing his knowledge of how PIV is done in typical dusty plasma experiments and for discussing its application to our experiment. We would also like to acknowledge the Rising Teacher program at LLNL, which allows future high school science teachers (in our case Brian Eberly) to participate in scientific research.

LLNL-XXX-XXXXXX. This work was performed under the auspices of the U.S. Department of Energy by Lawrence Livermore National Laboratory under Contract DE-AC52-07NA27344.

Facilities: Jupiter Laser Facility

REFERENCES

J. S. Mathis, W. Rumpl, and K. H. Nordsieck, Size distribution of interstellar grains, *Astrophys. J.* **217,** 425 (1977).

E. Herbst, Chemistry in the interstellar-medium, *Annu. Rev. Phys. Chem.* **46,** 27 (1995).

B. T. Draine and E. E. Salpeter, Destruction mechanims for interstellar dust, *Astrophys. J.* **231,** 438 (1979).

C. Gregory Seab and J. Michael Shull, Shock processing of interstellar grains, *Astrophys. J.* **275,** 652 (1983).

A. G. G. M. Tielens, C. G. Seab, D. J. Hollenbach, and C. F. McKee, Shock processing of interstellar dust: diamonds in the sky, *Astrophys. J.* **319,** L109 (1987).

C. F. McKee, D. J. Hollenback, C. G. Seab, and A. G. G. M. Tielens, The structure of time-dependent interstellar shocks and grain destruction in the interstellar medium, *Astrophys. J.* **318,** 674 (1987).

A. P. Jones, A. G. G. M. Tielens, D. J. Hollenback, and C. F. McKee, Grain destruction in shocks in the interstellar medium, *Astrophys. J.* **433,** 797 (1994).

D. A. Neufeld, S. Lepp, and G. J. Melnick, Thermal balance in dense molecular clouds: radiative cooling rates and emission-line luminosities, *Astrophys. J. Suppl. S.* **100,** 132 (1995).

A. P. Jones, A. G. G. M. Tielens, and D. J. Hollenback, Grain shattering in shocks: the interstellar grain size distribution, *Astrophys. J.* **469,** 740 (1996).

A. G. G. M. Tielens, C. F. McKee, C. G. Seab, D. J. Hollenbach, The physics of grain-grain collisions and gas-grain sputtering in interstellar shocks, *Astrophys. J.* **431,** 321 (1994).

R. S. Lewis, M. Tang, J. F. Wacker, E. Anders, and E. Steel, Interstellar diamonds in meteorites, *Nature* **326,** 160 (1987).

N. McBride, S. F. Green, and J. A. M. McDonnell, Meteoroids and small sized debris in low earth orbit and at 1 AU: results of recent modeling, *Adv. Space. Res.* **23,** 73 (1999).

G. A. Graham, A. T. Kearsley, M. M. Grady, I. P. Wright, A. D. Griffiths, and J. A. M. McDonnel, Hypervelocity impacts in low earth orbit: cosmic dust versus space debris, *Adv. Space Res.* **23,** 95 (1999).

M. J. Burchell, M. J. Cole, J. A. M. McDonnell, and J. C. Zarnecki, *Meas. Sci. Technol.* **10,** 41 (1999).

F. Horz, M. E. Zolensky, R. P. Bernhard, T. H. See, and J. L. Warren, Impact features and projectile residues in aerogel exposed on Mir, *Icarus* **147,** 559 (2000).

G. A. Graham, N. McBride, A. T. Kearsley, G. Drolshagen, S. F. Green, J. A. M. McDonnell, M. M. Grady, and I. P. Wright, The chemistry of micrometeoroid and space debris remnants captured on Hubble Space Telescope solar cells, *Int. J. Impact Eng.* **26,** 263 (2001).

G. A. Graham, A. T. Kearsley, G. Drolshagen, N. McBride, S. F. Green, and I. P. Wright, Microparticle impacts upon HST solar cells, *Adv. Space Res.* **28,** 1341 (2001).

G. A. Graham, A. T. Kearsley, I. P. Wright, M. J. Burchell, and E. A. Taylor, Observations on hypervelocity impact damage sustained by multi-layered insulation foils exposed in low earth orbit and simulated in the laboratory, *Int. J. Impact Eng.* **29,** 307 (2003).

G. A. Graham, P. G. Grant, R. J. Chater, A. J. Westphal, A. T. Kearsley, C. Snead, G. Dominguez, A. L. Butterworth, D. S. McPhail, G. Bench, and J. P. Bradley, Investigation of ion beam techniques for the analysis and exposure of particles encapsulated by silica aerogel: Applicability for Stardust, *Meteorit. Planet. Sci.* **39,** 1461 (2004).

J. T. Larsen and S. M. Lane, HYADES - A plasma hydrodynamics code for dense-plasma studies, *J. Quant. Spectrosc. Radiat. Transfer* **51,** 179 (1994).

J. G. Clérouin, M. H. Cherfi, and G. Zérah, The viscosities of dense plasmas mixtures, *Europhys. Lett.* **42,** 37 (1998).

H. F. Robey, Effects of viscosity and mass diffusion in hydrodynamically unstable plasma flows, *Phys. Plasmas* **11,** 4123 (2004).

B. R. Munson, D. F. Young, and T. H. Okiishi, *Fundamentals of Fluid Dynamics,* John Wiley & Sons, Inc. (2006).

http://jlf.llnl.gov

E. Thomas, Jr., Observations of high speed particle streams in dc glow discharge dusty plasmas, *Phys. Plasmas* **8,** 329 (2001).

Comet chasers get mineral shock, *Nature* **440,** 260 (2006).

G. A. Graham, N. Teslich, Z. R. Dai, J. P. Bradley, A. T. Kearsley, F. Horz, Focused ion beam recovery of hypervelocity impact residue in experimental craters on metallic foils, *Meteorit. Planet. Sci.* **41,** 159 (2006).

B. L. Holian and P. S. Lomdahl, Plasticity induced by shock waves in nonequilibrium molecular-dynamics simulations, *Science* **280,** 2085 (1998).

K. Kadau, T. C. Germann, P. S. Lomdahl, and B. L. Holian, Microscopic view of structural phase transitions induced by shock waves, *Science* **296,** 1681 (2002).

E. M. Bringa, A. Caro, Y. W. Wang, M. Victoria, J. M. McNaney, B. A. Remington, R. F. Smith, B. R. Torralva, and H. Van Swygenhoven, Ultra-Hard Nanocrystalline Metals by Shock Loading, *Science* **309,** 1838 (2005).